ACS Chemical Neuroscience

Research Article

Cite This: ACS Chem. Neurosci. 2018, 9, 3060−3071

pubs.acs.org/chemneuro

Oligomer Diversity during the Aggregation of the Repeat Region of Tau

Magnus Kjaergaard,[†,‡,#] Alexander J. Dear,[†,#] Franziska Kundel,[†,∇] Seema Qamar,[§] Georg Meisl,[†] Tuomas P. J. Knowles,[*,†,∥] and David Klenerman[*,†,⊥]

[†]Department of Chemistry, Cambridge University, Lensfield Rd, Cambridge CB2 1EW, United Kingdom

[‡]Aarhus Institute of Advanced Studies, Aarhus University, Høegh-Guldbergs Gade 6B, DK-8000 Aarhus C, Denmark

[§]Cambridge Institute for Medical Research, University of Cambridge, Hills Road, Cambridge CB2 0XY, United Kingdom

[∥]Cavendish Laboratory, Department of Physics, University of Cambridge, Cambridge CB3 0HE, United Kingdom

[⊥]UK Dementia Research Institute, University of Cambridge, Cambridge CB2 0XY, United Kingdom

Supporting Information

ABSTRACT: The molecular mechanism of protein aggregation is of both fundamental and clinical importance as amyloid aggregates are linked to a number of neurodegenerative disorders. Such protein aggregates include macroscopic insoluble fibrils as well as small soluble oligomeric species. Time-dependent resolution of these species is prerequisite for a detailed quantitative understanding of protein aggregation; this remains challenging due to the lack of methods for detecting and characterizing transient and heterogeneous protein oligomers. Here we have used single molecule fluorescence techniques combined with mechanistic modeling to study the heparin-induced aggregation of the repeat region of tau, which forms the core region of neurofibrillary tangles found in Alzheimer's disease. We distinguish several subpopulations of oligomers with different stability and follow their evolution during aggregation reactions as a function of temperature and concentration. Employment of techniques from chemical kinetics reveals that the two largest populations are structurally distinct from fibrils and are both kinetically and thermodynamically unstable. The first population is in rapid exchange with monomers and held together by electrostatic interactions; the second is kinetically more stable, dominates at later times, and is probably off-pathway to fibril formation. These more stable oligomers may contribute to other oligomer induced effects in the cellular environment, for example, by overloading protein quality control systems. We also show that the shortest growing filaments remain suspended in aqueous buffer and thus comprise a third, smaller population of transient oligomers with cross-β structure. Overall our data show that a diverse population of oligomers of different structures and half-lives are formed during the aggregation reaction with the great majority of oligomers formed not going on to form fibrils.

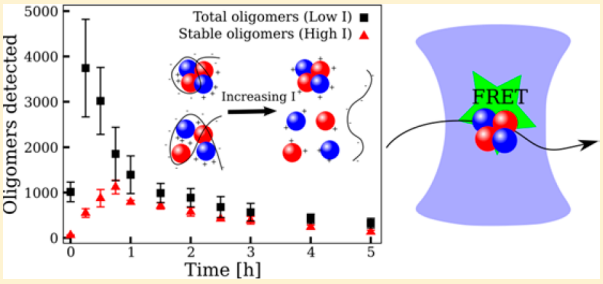

KEYWORDS: *tau, amyloid oligomers, single-molecule FRET, kinetic modeling, aggregation mechanism*

Assembly of proteins into large insoluble fibrils is a characteristic hallmark, and possibly a cause, of several neurodegenerative diseases such as Parkinson's and Alzheimer's diseases.[1] In Alzheimer's disease, two distinct types of protein aggregates are found in the brain *post mortem*: extracellular plaques composed of the amyloid-β peptide and neurofibrillary tangles composed of the protein tau. Of these two types of fibrils, the neurofibrillary tangles correlate more strongly with the extent of pathology, leading to an interest in the mechanism of their formation.[2]

Tau is an intrinsically disordered protein that is thought to bind and stabilize microtubules, thus assisting intracellular transport.[3] The microtubule binding site is located in the C-terminal half of the protein and contains three or four repeats with high β-sheet propensity, which form most of the core of the neurofibrillary tangles.[4,5] As this repeat region contains the regions required for filament formation, it is widely used for biophysical studies of the aggregation of tau. The repeat region is also the site of a number of point mutations, such as ΔK280 and P301L, which both cause early onset frontotemporal dementia.[6,7] *In vitro* aggregation of tau is slow as the repeat region is highly positively charged, leading to intermolecular repulsion. This repulsion can be overcome to trigger aggregation, which has been suggested to occur either by excessive phosphorylation of tau or by addition of negatively charged cofactors such as RNA or heparin sulfate.[8,9]

In addition to neurofibrillary tangles, tau can form a range of oligomeric forms with different properties. Oligomers of amyloid forming proteins are heterogeneous and rare relative to the monomer and fibrillar forms. This complicates the

Received: May 25, 2018
Accepted: June 28, 2018
Published: June 28, 2018

DOI: 10.1021/acschemneuro.8b00250
ACS Chem. Neurosci. 2018, 9, 3060−3071

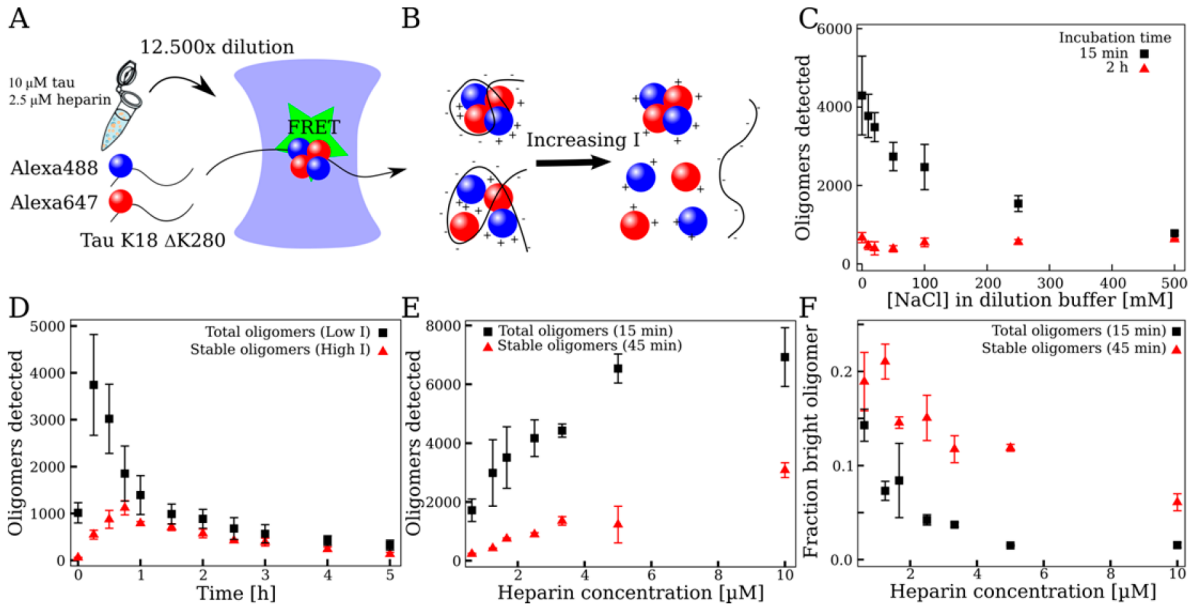

Figure 1. (A) Sketch of molecule assay for detection of oligomers. The experiments use tau K18 ΔK280 labeled just outside the amyloidogenic core with either Alexa488 or Alexa647 in equal amounts. The dyes are excited with a diffraction limited 488 nm laser spot and detected one by one in a microfluidic flow channel using a confocal microscope. (B) The need for heparin to initiate the reaction suggests a dependence on electrostatic interactions. The ionic strength of the dilution buffer can thus be used to discriminate between oligomers with differential dependence on electrostatic interactions with heparin. (C) Samples from an early (15 min) and a late (2 h) time point in an aggregation reaction were diluted into buffers with different ionic strength. The number of observed oligomers decreases dramatically for the early time point, whereas the late time point is independent of ionic strength. (D) Samples are taken from an aggregation reaction at 37 °C and diluted into a dilution buffer with either 500 mM NaCl or no NaCl. The number of oligomers detected at low ionic strength peaks at the first time point but drops rapidly to similar numbers as that observed at high ionic strength suggesting initial formation of electrostatically stabilized oligomers in kinetic experiments. (E) The number of oligomers detected increases with increasing heparin concentration, where there is a decrease in the fraction of bright oligomer events (F) (defined as bursts with more than ten times the photons of an average monomer burst). This suggests that higher heparin concentration leads to more and smaller oligomers. Error bars represent SEM from three repeats.

characterization of oligomers, especially the transient species occurring during fibrillation that cannot be purified. In cases where oligomers have been characterized, a range of species coexist. For example in the case of α-synuclein, oligomers fall into two broad classes, where globular oligomers are formed initially and gradually convert into cytotoxic oligomers with amyloid-like cross-β structure.[10] These oligomers include different segments of the protein chain,[11] differ in population between pathological mutants,[12] and undergo two unimolecular conversion steps before fibrillation.[13] For many amyloidogenic proteins, both the monomers and the fibrils are not particularly toxic to cells, which is also the case for tau. The cytotoxic agents are thus typically soluble oligomeric aggregates.[14] Due to the heterogeneity of oligomers only some of these oligomers can grow into fibrils, and only some are cytotoxic.

We recently developed a single molecule Förster resonance energy transfer (smFRET) assay detecting tau oligomer populations during filament formation.[15] We showed that tau oligomers are populated at low concentrations during the aggregation reaction and require an intramolecular conversion step before growth into filaments. Mutants associated with frontotemporal dementia have much higher oligomeric populations, primarily due to faster oligomer formation. In previous studies of α-synuclein using the same methodology,[10,12,13] we observed two populations of oligomers based on FRET efficiency, which had different stabilities. In our previous studies of tau, we did not observe distinct FRET populations.[15] In this study, we revisit single molecule FRET studies of tetra repeat (K18) tau aggregation by using the buffer conditions to resolve species of different stabilities. Where possible, we determine the activation barriers for the key reactions and gain insight into the range of oligomers formed during aggregation using detailed mechanistic models fitted over a range of temperatures and concentrations.

RESULTS

Single-Molecule Techniques Identify Three Different Classes of Oligomers. To monitor rare oligomeric species during the aggregation reaction, we use an engineered tau labeled with a single fluorophore per molecule. By mixing aliquots labeled with different dyes, we ensure that half of the tau molecules are labeled with a FRET donor and half with a FRET acceptor. Monomeric tau shows no FRET, but in oligomers, the fluorophores are brought into close proximity and FRET occurs (Figure 1A). It should be noted that the labeling requires us to remove the two native cysteines in K18 tau, and thus we do not observe the disulfide bond formation suggested to affect some forms of *in vitro* aggregation reactions. The FRET is detected one particle at a time using a confocal single molecule FRET instrument. This allows us to simultaneously quantify populations of oligomers in a vast excess of monomeric tau.[16] The oligomeric population of wild-type K18 tau is low and close to the limit of detection for this assay; however the pathological mutation ΔK280 gave rise to higher oligomer concentrations that can be quantified robustly. In our previous study, we verified that the fluorophore labeling only minimally affected the kinetics of the process and the

DOI: 10.1021/acschemneuro.8b00250
ACS Chem. Neurosci. 2018, 9, 3060−3071

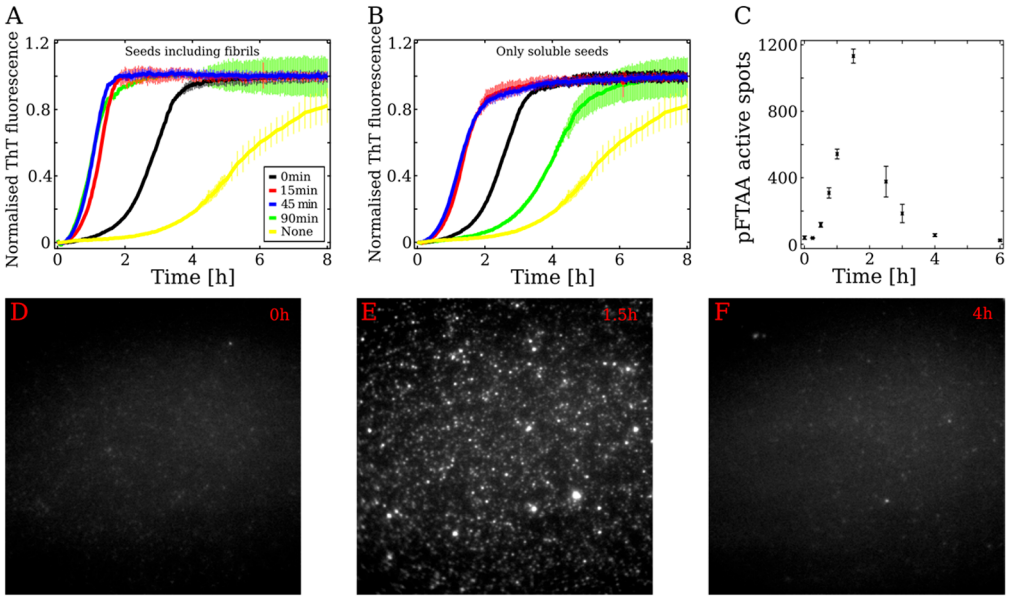

Figure 2. Seeding and single oligomer imaging using an amyloid-specific dye. (A) To allow observation of the effect of seeding, the aggregation reaction was slowed down by reducing the temperature (30 °C) and changing the buffer conditions. Aliquots of the reactions were taken at different time points of the reaction, similar to Figure 1D, and added to a fresh reaction (10% volume). The aliquots were taken from either the whole solution (A) or a solution cleared of larger fibrillar species by centrifugation (B). The reaction mixture effectively seeds the new reaction, although the number of smaller fibrillar seeds decrease after an initial peak. (C−F) Aliquots were taken at different time points from a reaction of K18 tau ΔK280 (10 μM tau, 37 °C, 1:4 heparin/tau) and adsorbed to a cover slide. The amyloid-like species were imaged using TIRF microscopy with the amyloid specific fluorophore pFTAA. The time course (C) shows a gradual build-up and eventual disappearance of particles with cross-β structure. Error bars represent SEM from three repeats.

morphology of the filaments formed.[15] We therefore used this mutant as a model system for studying events occurring in tau oligomers.

The single molecule FRET assay has previously shown that different classes of oligomers of synuclein could be distinguished based on shifting FRET efficiencies.[10] Tau K18 displayed a broad FRET peak with no clear development during the reaction[15] suggesting that another strategy is needed to separate any putative different species of tau oligomers. Single molecule FRET detection of oligomers requires dilution to the picomolar level, well below the concentrations needed to sustain a fibrillation reaction (Figure 1A). This approach only detects oligomers that are stable during the duration of the measurement (6 min). The low concentrations used therefore pose both a challenge to detecting transient oligomers, and an opportunity to use differential stability to distinguish oligomer populations. We speculated that we could tune the dilution buffer to destabilize certain species causing them to dissociate before detection.

K18 tau requires the addition of a cofactor for efficient *in vitro* aggregation, usually polyanions such as RNA or heparin.[17,18] The polyanionic nature of the cofactors suggests that their role is to help cationic tau overcome charge−charge repulsion, for example, by electrostatically assisting oligomer formation and thus seeding the reaction. This suggests that ionic strength provides a promising way to distinguish different subpopulations of oligomers, by selectively destabilizing heparin-dependent oligomers with high ionic strength. To test this hypothesis, we diluted samples from an aggregation reaction into buffers with either higher or lower ionic strength than the reaction conditions (Figure 1B). It should be noted that while we record the FRET data under extreme conditions of ionic strength in order to distinguish high- and low-stability oligomers, the reaction conditions where the oligomers are formed is near physiological ionic strength. We found that early tau oligomers, which can be detected after 15 min of aggregation,[15] disassociated with increasing ionic strength, while later oligomer populations are largely independent of ionic strength (Figure 1C). At physiological ionic strength, we still detected a considerable population of the electrostatically stabilized oligomers, suggesting that these could play a role *in vivo*.

The dependence of oligomer stability on buffer conditions showed that the dilution buffer can be used to separate different classes of oligomers in kinetic experiments. Therefore, we performed aggregation reactions where the aliquots were diluted in either high (containing 0.5 M NaCl) or low ionic strength buffer (no NaCl). When the reaction mixture was analyzed in low ionic strength buffer, the oligomer population peaked at the first time point and subsequently decayed (Figure 1D). When the reaction was analyzed in high ionic strength buffer, the oligomer population is smaller and built up slowly to a peak after 45 min. Notably, the oligomer populations converged at later time points, showing that the population shifts to more stable oligomers that cannot be disassociated in high ionic strength buffer. This implies the presence of a population of electrostatically stabilized oligomers early in the reaction that later gives way to more stable species, presumably stabilized through hydrophobic interactions. In the following, we refer to the oligomers that do or do not depend on electrostatic interactions as type A and B oligomers, respectively. We may estimate the concentrations of these oligomer populations directly by comparing the burst rates to samples of labeled tau at known concentrations. We determined the concentration of type A oligomers by

DOI: 10.1021/acschemneuro.8b00250
ACS Chem. Neurosci. 2018, 9, 3060−3071

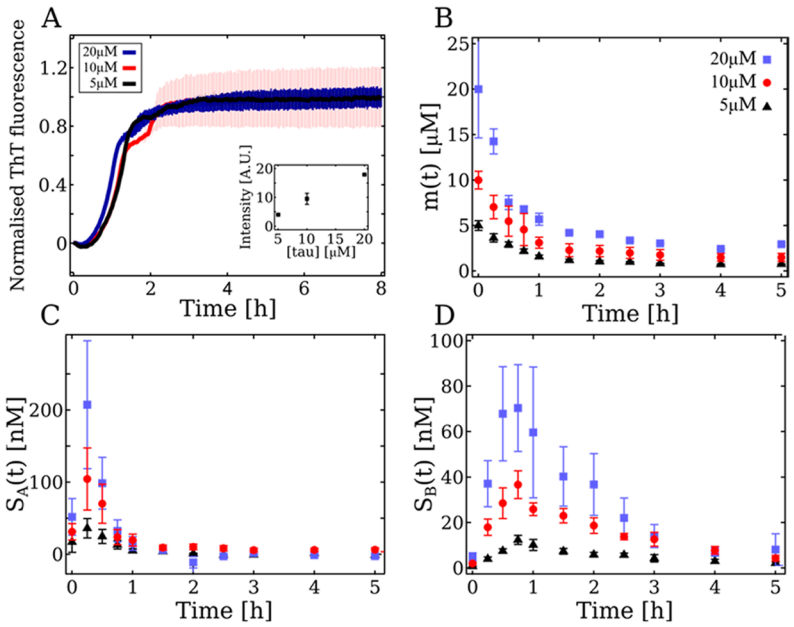

Figure 3. Concentration dependence of tau K18 ΔK280 aggregation. (A) ThT assay of K18 tau ΔK280 at different tau concentrations with 1:4 heparin/tau ratio. (B–D) Single-molecule FRET experiments were used compare aggregation reactions run at different concentrations of tau (1:4 heparin/tau). Based on burst rates, we estimate the concentrations of monomeric tau (B), type A oligomers (C), and stable type B oligomers (D). The populations of the different species evolve with similar time constants in the different experiments, and the oligomer population roughly scales with the total monomer concentration. Error bars represent SEM from three repeats.

subtracting the concentration of type B oligomers from the total concentration.

If the type A oligomers are indeed nucleated by direct interactions with the anionic cofactors, then the oligomer ensemble should be sensitive to the ratio of tau and heparin. We tested this by performing aggregation experiments with varying heparin/tau ratios. In ThT monitored reactions at different heparin/tau ratios, the final amount of ThT positive aggregates scales with the heparin concentration, although there is no appreciable effect on the half-life (Figure S1). The population of tau oligomers increases with increasing heparin concentration although it reaches a plateau around a ratio of 1:2 (Figure 1E). This ratio corresponds to the fastest fibril formation rate in previous studies.[19] With increasing heparin concentration, the average size of oligomers decreased for both transient and stable oligomers, which is shown by the reduced fraction of oligomers above a given brightness threshold (Figure 1F). These results show that heparin participates directly in the formation of early oligomers and that both type A and type B oligomers are present in a range of sizes.

Filaments generated in aggregation reactions are present in a range of lengths and can form a colloidal suspension. Species detectable by smFRET that meet the IUPAC definition of oligomers therefore include short elongation-competent filaments ("fibrillar oligomers")[20] as well as possible prefibrillar intermediates of nucleation. In our experiments, we have identified two distinct classes of oligomers (types A and B). Combining average fibril lengths derived from TEM (~2000 monomers)[15] with the total amount of tau incorporated into fibrils based on monomer depletion data (~8.5 μM), we estimate that the final fibril concentration (~4.25 nM) is far lower than the maximum observed concentrations of either oligomer class (e.g., 104 and 37 nM at 37 °C for types A and B, respectively), which must therefore both be distinct prefibrillar intermediates. Fibrillar oligomers must thus comprise a third class of oligomer in this system. They are likely to be stable and thus detected with the type B oligomers in the FRET assay; however, since their concentration is comparatively negligible, the measured type B oligomer concentration effectively corresponds to prefibrillar oligomers. Furthermore, almost all type A and B oligomers are depleted by the end of the reaction, therefore most of them must dissociate or otherwise deplete rather than becoming fibrils.

Oligomeric species may be on and some off the main reaction pathway to insoluble fibrils. On-pathway intermediates should shorten the lag phase in aggregation reactions by circumventing part of the nucleation process. The lag phase of tau K18 ΔK280 is absent under the conditions used for smFRET experiments, so to study the effect of seeding, we changed ionic strength and temperature to lengthen the lag phase to 4 h (Figure 2A). The seeds were drawn from an aggregation reaction identical to that used in Figure 1, and added to a fresh reaction at slower aggregation conditions. It should be noted that all time points were drawn from the same reaction and that early samples were stored on ice until analysis. The assumption behind this experimental design is that there is little development in the oligomer population during the incubation on ice. All seeding samples shorten the lag phase dramatically (Figure 2A,B), and the effect is almost identical regardless of whether the seeding sample is taken after 15, 45, or 90 min, despite the aggregation reaction being almost complete by 90 min. This demonstrates that elongation-competent fibrillar species are responsible for the observed seeding effect and that most fibrillar seeds are formed almost instantaneously after addition of heparin, such that nucleation of new filaments ceases after very early times. The seeding reaction was then repeated where larger aggregates were removed from the seeding solution by centrifugation. The early time points have a similar ability to seed fibril formation (Figure 2B), but most of the growth competent fibrils are

DOI: 10.1021/acschemneuro.8b00250
ACS Chem. Neurosci. 2018, 9, 3060–3071

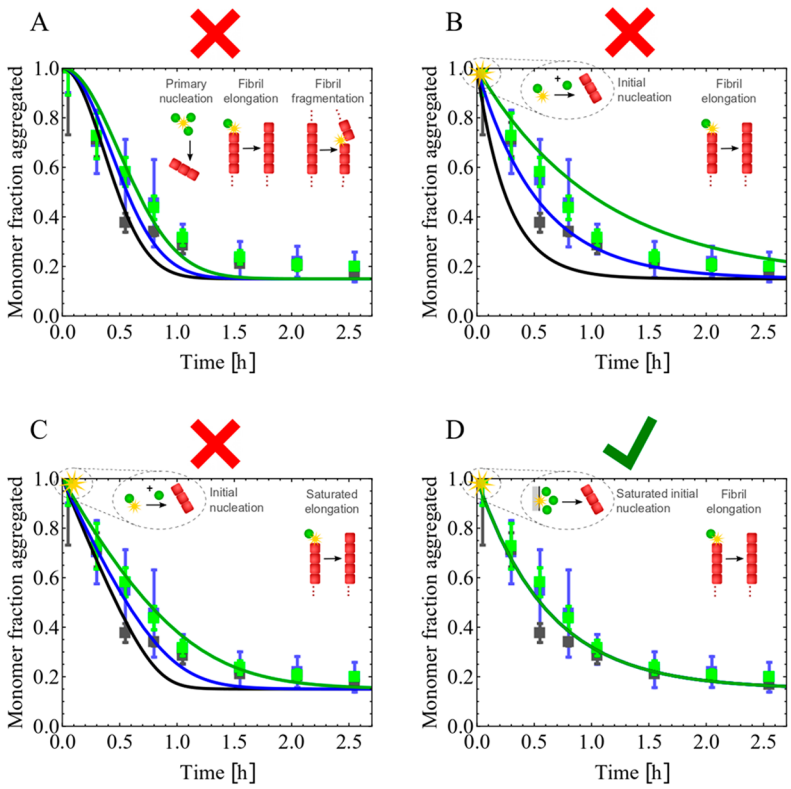

Figure 4. Testing different bulk kinetic models reveals the mechanism of filament formation. (A) Traditional models of biofilament formation cannot reproduce the data; misfits reveal the absence of secondary processes and of a conventional primary nucleation step. (B) Using the "initial nucleation" mechanism inferred from the seeded experiments captures the curve shape but overestimates the concentration dependence of the aggregation. (C) Allowing saturation of the elongation reaction step cannot match the concentration dependence while retaining the correct curve shape at late times. (D) Allowing instead the "initial nucleation" process to be fully saturated yields good fits. The equations for the misfit models are given in the SI, in addition to an outline of model selection theory and estimation of fit quality. Initial monomer concentrations: black, m_0 = 20 μM; blue, m_0 = 10 μM; green, m_0 = 5 μM.

removed at later time points. This demonstrates that most fibrillar species are small enough at early time points to still be suspended after centrifugation; it is therefore reasonable to label them fibrillar oligomers.

Previous studies of amyloid forming proteins have shown the coexistence of oligomers with and without a cross-β structure.[10] To test whether this is the case for the tau oligomers observed here, we used a recently developed assay (SAVE)[21,22] that allows single aggregate detection of the fluorescence from an amyloid specific dye. Aliquots were taken during the reaction of tau, and oligomers were adsorbed on a glass surface. Oligomers were detected *via* the amyloid specific dye pFTAA[23] and total internal reflection fluorescence (TIRF) microscopy (Figure 2C–F). pFTAA has been demonstrated to recognize a range of earlier intermediates of amyloidogenic proteins and was thus preferred over the more traditional ThT. The population of oligomers builds up to a peak concentration and gradually disappears (Figure 2C). Notably, this oligomeric population has a different kinetic profile than either the type A or type B oligomers, showing that it represents a third species. Fibrillar oligomers have a high cross-β content, so they are likely the species being reported here. It should, however, be noted that due to the adsorption to a glass surface in this experiment, larger oligomers are likely preferentially detected, and so the population of this species cannot be accurately quantified. Therefore, we do not include this third class of oligomers in the subsequent modeling.

Heparin-Mediated Tau Fibril Formation Proceeds *via* an Unusual Mechanism. The aggregation kinetics of many amyloid-forming peptides have been modeled over the past two decades, with formation of new fibrillar species from soluble peptide usually treated as a single coarse-grained nucleation reaction step.[24−26] In all these models, fibrillar species undergo rapid growth by monomer addition ("elongation"). The difference in time scales between nucleation and elongation gives rise to extended fibrils.

To permit global fitting,[27] we varied the concentration of tau in the aggregation reaction at a heparin/tau ratio of 1:4. Bulk ThT fluorescence experiments yielded identical normalized reaction trajectories (Figure 3A). This implies that the rate of new filament formation is independent of the monomer concentration. We repeated these experiments with the single molecule FRET assay and diluting the aliquots into high and low ionic strength buffers as above. This thus allowed us to follow the concentrations of monomeric tau (Figure 3B), type A oligomers (Figure 3C), and type B oligomers (Figure 3D) during the reaction. Similarly to the bulk assays, the reaction trajectories of monomers and both types of oligomers deduced from single molecule observations superimpose when normalized by the initial monomer concentrations. The seeding experiment described above provides evidence that fibril nucleation occurs almost instantaneously at the start of the reaction and then ceases. By testing a series of bulk aggregation models (Figure 4), we verified that the only simple

DOI: 10.1021/acschemneuro.8b00250
ACS Chem. Neurosci. 2018, 9, 3060−3071

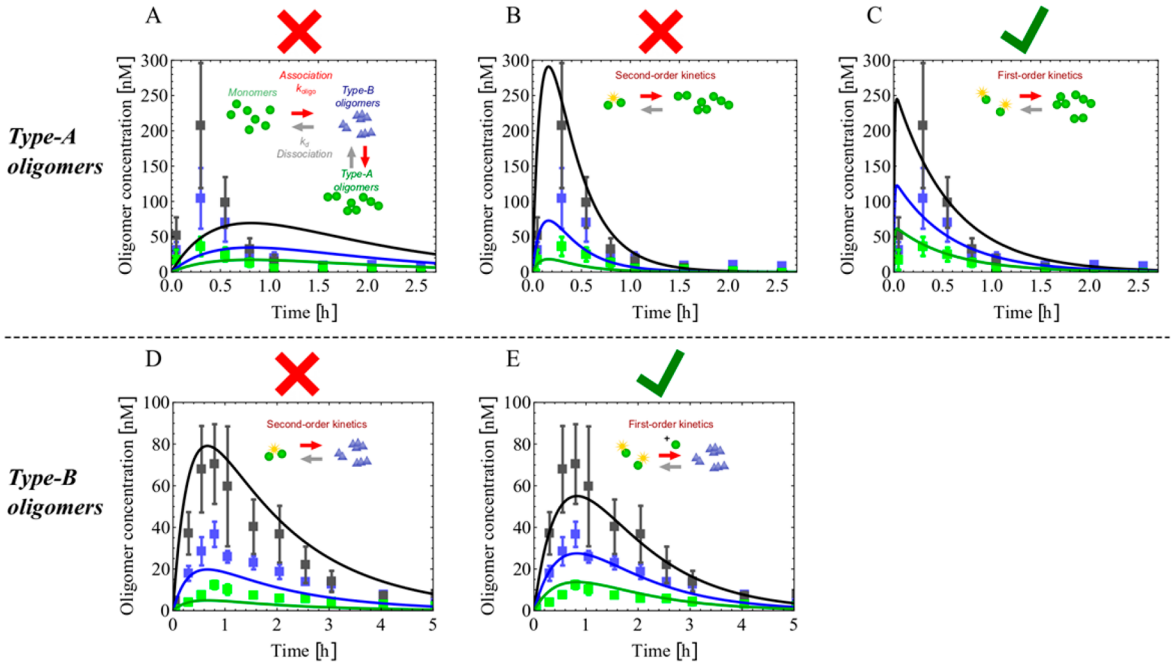

Figure 5. Testing of different oligomer kinetic models reveals the mechanisms of oligomer formation. (A–C) Type A oligomers are found to form very rapidly, directly from monomers; the formation step is partially saturated with a reaction order of 1. (D, E) Type B oligomers form from the reactant ensemble of monomers and type A oligomers with a reaction order of 1. The equations for the misfit models are given in the SI, in addition to an outline of model selection theory and estimation of the fit quality. Initial monomer concentrations: black, m_0 = 20 μM; blue, m_0 = 10 μM; green, m_0 = 5 μM.

kinetic model capable of reproducing the monomer reaction trajectory to within most of the error bars is such an "initial nucleation" model similar to that described previously for an unrelated protein.[28] We further verified that the number of fibrils formed at the start of the reaction is independent of the initial monomer concentration and is thus likely mediated by a surface, for instance, the air–water interface. In such a scenario, the rate-limiting factor would be the availability of the interface, resulting in no monomer dependence for the nucleation rate. Furthermore, the ceasing of nucleation after an early time could represent a lack of availability of free interface at later times.

Finally, we were able to infer (see SI) that the fibril disaggregation rate is negligible, and the monomeric tau remaining at the end of the reaction is inactive and unable to aggregate into fibrils, possibly due to changes in heparin stoichiometry during the reaction. With insufficient data to determine exactly why this occurs, we do not explicitly model this inactive monomer population.

Characterizing the Kinetics of Tau Oligomers. We previously proposed a minimal kinetic model of K18 tau aggregation involving formation of a population of growth incompetent prefibrillar oligomers that convert into growth competent fibrillar species.[15] With the expanded data set recorded here, we thus sought to elaborate on this model, through quantitative modeling of the time evolution of monomeric, oligomeric, and fibrillar species. Having determined the mechanism of fibril formation, we next tested a series of mechanisms featuring different reaction steps between the oligomeric species (Figure 5), to eliminate inconsistent mechanisms and uncover the most likely ones for quantitative analysis (see SI for outline of model selection theory).

We first demonstrated that type A oligomers form directly from monomers and dissociate so rapidly that they are almost at equilibrium with monomers on the measurement time scale of our experiments, especially at higher temperatures. We further showed that the reaction order of type A oligomer association with respect to monomers is unity. Note the reaction order is not in general the same as the critical nucleus size;[27,29] its value here indicates a saturation effect, possibly due to association occurring at surfaces.

The saturated nature of the new filament formation process meant it was not possible from the kinetic data to determine conclusively whether type B oligomers were on-pathway to filament formation; however, given that the kinetics of type B oligomer formation appear substantially slower than those of filament formation, it seems unlikely that they are on-pathway.

The rapidity of exchange between monomers and type A oligomers relative to the time scale of monomer depletion prevented us from determining whether type B oligomers are formed directly from monomers or from conversion of type A oligomers. Indeed, from a kinetic modeling perspective it is more appropriate to treat monomers and type A oligomers as an ensemble of reactant species, rather than considering type A oligomers as an intermediate species.[30] Whether type A oligomers are on-pathway intermediates of type B oligomer formation is therefore not a meaningful question under these conditions, as the type A oligomers are part of the reactant ensemble. We therefore instead modeled the total flux of type B oligomers from monomers. The reaction order of formation of type B oligomers with respect to monomers was then found to be unity.

Quantitative Modeling. The minimal coarse-grained kinetic model capable of reproducing the time evolution of all the species we observe has been established above. The two

DOI: 10.1021/acschemneuro.8b00250
ACS Chem. Neurosci. 2018, 9, 3060–3071

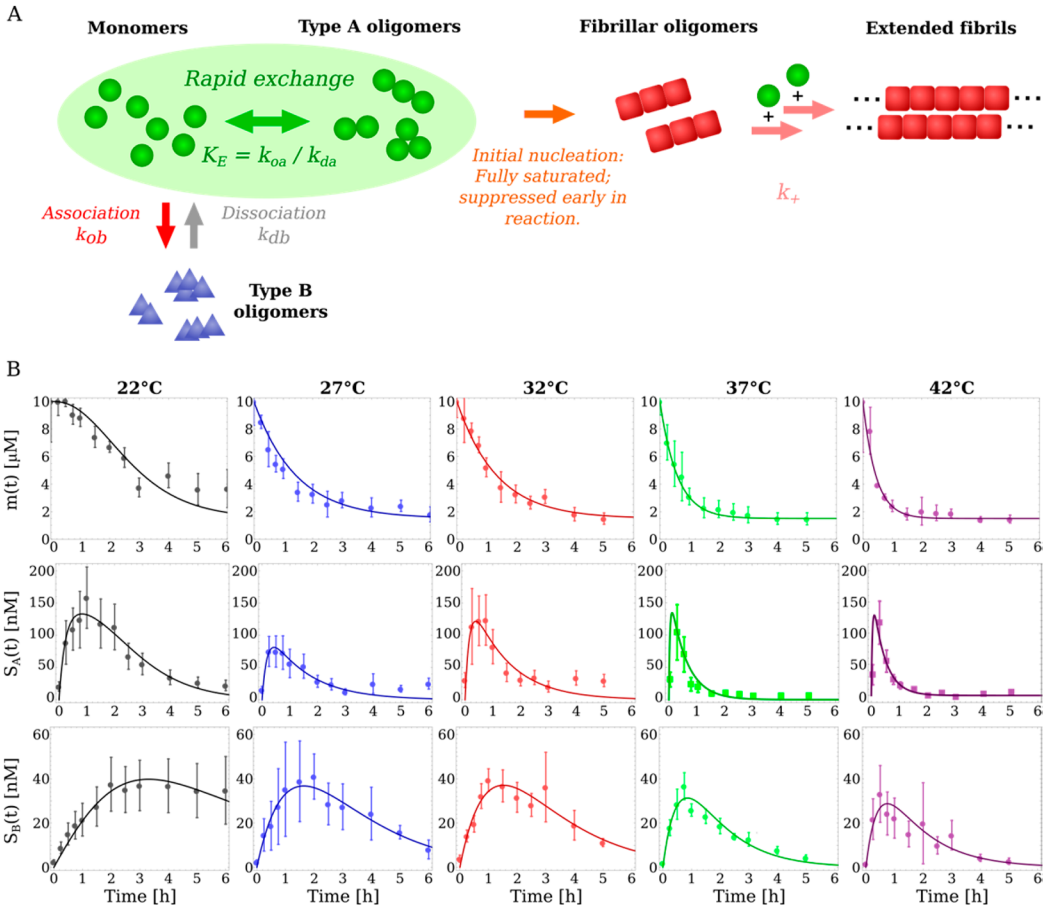

Figure 6. Modeling of the aggregation reaction based on temperature-dependence of the aggregation reaction. (A) The simplest model that describes the total data set involves a probable off-pathway, stable "type B" oligomer and an unstable "type A" oligomer in rapid exchange with the monomeric state. (B) Numerical fitting of concentration of monomers and the two classes of oligomers estimated from the single molecule aggregation assay. The model adequately describes the total data set and allows us to extract the thermodynamic parameters found in Table 1.

oligomer species, S_A and S_B, form through monomer association with rate constants k_{oA} and k_{oB} and disappear with rate constants k_{dA} and k_{dB}. Fibrils all form effectively instantaneously at the start of the reaction, yielding a constant fibril concentration [P]; these fibrils grow by monomer addition with rate constant k_+. The model explicitly considers the concentration of tau monomers $[m](t)$, the concentrations of oligomers $[S_A](t)$, and $[S_B](t)$, and the mass concentration of fibrils $[M](t)$.

Rate equations describing the system can be written as follows:

$$\frac{d[S_A](t)}{dt} = k_{oA}[m](t) - k_{dA}[S_A](t) \quad (1)$$

$$\frac{d[S_B](t)}{dt} = k_{oB}[m](t) - k_{dB}[S_B](t) \quad (2)$$

$$\frac{d[m](t)}{dt} = -2k_+[m](t)[P] \quad (3)$$

$$[m](t) + [M](t) = [m](0) \quad (4)$$

These equations may be solved analytically (see Methods). In principle, further complexity could be added to this coarse-grained kinetic modeling framework, for instance, differentiating between additional hypothetical subpopulations of oligomers or explicit modeling of heparin concentration; this would, however, require greater experimental constraints than currently available, to avoid overfitting. The purpose of the kinetic modeling is instead to discover the dynamical relationships between those coarse-grained species that our experiments are capable of resolving.

Using this model, we sought to characterize the temperature dependence of the aggregation reaction. We used the single molecule aggregation experiment to follow the populations of monomers and of the two different categories of prefibrillar oligomers formed during aggregation reactions from 22 to 42 °C (Figure 6). The temperature series extends slightly beyond physiologically relevant temperatures in both directions; however, this is necessary to determine the activation energies of the underlying reaction steps. To do so requires that only the rate constants change over this temperature range and not the reaction mechanisms. This is justified by the relatively narrow temperature range and validated by our successful global fitting of a single model across many temperatures and concentrations.

The data at 27 °C and above may be fitted to the integrated rate laws to determine the rate parameters in Table S1. However, at 37 and 42 °C, the exchange between monomers and type A oligomers is too rapid to determine the magnitudes of k_{oA} and k_{dA}; instead, only their ratio (equilibrium constant $K_E = k_{oA}/k_{dA}$) may be determined with any accuracy, averaged

DOI: 10.1021/acschemneuro.8b00250
ACS Chem. Neurosci. 2018, 9, 3060−3071

over these two temperatures (see Methods). Finally, at 22 °C a classical lag phase in the monomer depletion kinetics appears, and we must explicitly include the formation of new filaments in the model in order to reproduce this effect (see Methods). The kinetic equations for oligomers remain unchanged, and we may still directly compare the oligomer formation and dissociation rate constants across temperatures. Examining the data, we see that the reaction rates all tend to increase with temperature, as expected. The population at 27 °C of type A oligomers appears anomalously low, resulting in an anomalously low k_{oA} and K_E.

Similarly to protein folding,[31,32] a simplified view of the dynamics of protein aggregation may be arrived at by considering the individual reaction steps as diffusion processes across free energy landscapes. Kramers' theory[33,34] then provides an expression for each rate constant k in terms of the highest free energy barrier $\Delta G^{\ddagger\ominus}$ on the lowest possible free energy pathway crossing the landscape between the relevant reactants and products:

$$k = A \exp(-\Delta G^{\ddagger\ominus}/RT)$$

where T is the temperature, R is the gas constant, and A is a prefactor.

A has previously been estimated for the filament elongation reaction step by considering the peptide as a Gaussian polymer diffusing across a free energy surface.[35] It is given as $A = Dr_{eff}$, where D is a characteristic diffusion constant for polypeptides,[36] equal to 5×10^{-10} m^2 s^{-1}, and r_{eff} is a characteristic distance related to the curvature of the free energy surface, given by 2×10^{-11} m for tau K18. Note that a highly accurate value for A is not needed to determine free energies from rate constants since errors in the prefactor enter only logarithmically. The same estimate generalized for application to nonunity reaction orders was shown to be a reasonable approximation for A for the other reaction steps of protein aggregation.[37]

Given this estimate for the prefactor ($A = 2 \times 10^4$ μM^{-1} h^{-1}) and rate constants over a range of temperatures, we may estimate both enthalpies and entropies of activation. We were able to extract enthalpies and entropies of activation for elongation, k_+ based on rate constants from 27−42 °C, and oligomer type B formation, k_{oB} and k_{dB}, using the entire temperature series (Table 1). The rate constants of oligomer type A formation, k_{oA} and k_{dA}, cannot be determined with sufficient accuracy to permit a thermodynamic analysis of the energy barrier. To estimate k_+, we used an average fibril length, L, of ∼2000 monomers per fibril as estimated previously from TEM.[15] Dividing the mass concentration of fibrils formed by this value yields [P], which is unlikely to have a significant temperature dependence, since it is likely surface-limited. In turn, this permits extraction of a temperature-dependent k_+. Any errors in L only affect the results of the barrier analysis logarithmically.

Table 1. Thermodynamic Parameters Extracted from Modeling

rate constants	H (kJ/mol)	TS (37 °C) (kJ/mol)	G (37 °C) (kJ/mol)
k_+	69 ± 7	56 ± 7	12 ± 1
k_{oB}	55 ± 5	17 ± 5	37 ± 1
k_{dB}	46 ± 17	19 ± 17	27 ± 1

DISCUSSION

Using single particle approaches, we have identified and characterized three major categories of oligomers formed during the aggregation of K18 tau. It is unlikely that this represents the full diversity of oligomers, however, as some classes of oligomers may be too rare to be detected or will be lumped together in our measurements. Several studies have previously demonstrated significant heterogeneity in the oligomers formed by amyloidogenic proteins. This heterogeneity translates into differences in functional properties such as toxicity.[38,39] Notably, a recent study of the yeast prion protein Ure2 demonstrates the formation of two separate oligomer species with different kinetic and structural properties. Similar to our results, both of these oligomers are unstable and predominantly dissociate; unlike our study, however, both are positively identified as on-pathway to fibril formation.[40] Previous studies of tetrarepeat tau aggregation have also suggested the existence of stable off-pathway oligomers, which were found to resemble short rod-like protofibrils.[41] This study also suggested the existence of heparin-stabilized oligomers, that are both in rapid exchange with monomers and on-pathway to fibrils. While numbers are not directly comparable due to differences in the reaction conditions, this model is qualitatively similar to the one we propose here. The advantage of the approach taken here is that we can follow the appearance and eventual fate of the different oligomeric species and thus use these data for mechanistic modeling. These models revealed that the most frequently occurring oligomer is transient in nature. A significant energetic rearrangement would be needed for these to convert to growth-competent, fibril-like oligomers, which are present at far lower concentrations. These initial transient oligomers are replaced by more stable type B oligomers, that seem to be off-pathway to fibril formation. The kinetics of oligomer formation observed in the SAVE experiment is slower than that observed by FRET, and therefore, this experiment likely reports on a separate group of oligomers not separated in our FRET experiments due to their lower incidence. Given that the SAVE experiment is believed to report on cross-β structure, the difference in kinetics observed between the different experiments suggest that the type B oligomers do not have the mature cross-β structure.

Several other groups have estimated activation enthalpies of the different steps of the fibrillation process. Typically, these estimations have been done from bulk studies and determine the energy barriers of nucleation and of elongation. Comparatively few, however, have estimated transition state entropies. We calculate both the enthalpy and the entropy of activation for elongation, and find they are of a similar magnitude to those reported in other proteins.[42] The moderately large enthalpic barrier is likely due to breakage of hydrogen bonds and other interactions associated with solvation and with internal structure, and the highly favorable transition state entropy is likely due to desolvation of hydrophobic segments of the monomer and the fibril end.

It is difficult to infer the energy barriers to formation and depletion of prefibrillar oligomeric intermediates in bulk studies, as oligomer formation is accompanied by the subsequent appearance of fibrils that dominate bulk measurements. A major advantage of the present study is that the quantitative observation of individual oligomer populations permits the decomposition of such rates, and we thus report

DOI: 10.1021/acschemneuro.8b00250
ACS Chem. Neurosci. 2018, 9, 3060−3071

the kinetic and thermodynamic signatures of formation of two oligomeric species formed in parallel. In agreement with other studies on filament nucleation, we find that the type B oligomer formation reaction has an enthalpic barrier of 55 kJ/mol but is driven by a small favorable entropic contribution to the transition state. The type A oligomer formation and depletion free energy barriers are too low to be characterized under present conditions. Studies of the nucleation of $A\beta_{1-42}$ indicate a much larger enthalpy of activation of 144 kJ/mol.[37] If the mechanism of tau oligomer formation is typical of amyloidogenic peptides, this would imply that fewer rearrangements and loss of bonds to solvent are needed for amyloid oligomer formation than for fibril formation and that the main enthalpic barrier for fibril nucleation lies in the conformational conversion step that transforms on-pathway oligomers to growing fibrils. The enthalpy of activation of tau oligomerization is instead approximately of the same magnitude as elongation by one monomer for other amyloid-forming proteins, which in a large systematic study was found to range from 27 to 107 kJ/mol for proteins without a rigid tertiary structure.[42] The transition state is unlikely to solely involve dissociation of heparin, whose enthalpy of binding to tau is −6 kJ/mol.[43] Given its similarity to enthalpic barriers for elongation, it probably instead predominantly consists of breaking intraprotein and protein−solvent interactions. Candidates for such intramolecular interactions have been identified by NMR spectroscopy, which shows both transient local and long-range structure in both K18 and full-length tau.[44−46] The favorable entropy term for the type B oligomer formation transition state is significantly smaller than that for elongation and moreover is approximately symmetrical with respect to dissociation, suggesting that it is not due solely to desolvation of hydrophobic regions of the peptides. Combined with the $n = 1$ reaction order, we infer that the highest transition state associated with the barrier represents a conformational rearrangement, either of heparin-bound tau monomer or of a type A oligomer (the latter possibly involving heparin dissociation) and not the association of two monomers.

Our results show that primary nucleation is saturated with respect to monomer and ceases rapidly as the reaction progresses. A simple physical mechanism, which can result in such behavior, is heterogeneous nucleation at surfaces. This type of behavior has been found to dramatically enhance the primary nucleation of new amyloid filaments from some important peptides.[28,47,48] Furthermore, similar behavior has been observed for tau *in vitro*[49] and suggested to occur *in vivo*.[50] An avenue for future research would be to test this explanation by varying the properties of the interfaces in the experimental setup. Microdroplet-based aggregation experiments would permit particularly fine control of the interfaces.[51,52]

Due to the heterogeneity of the aggregate species assembled from amyloidogenic proteins, it is usually difficult to assign specific functions to certain classes of aggregates. Information may be inferred by comparing the physiological effects of samples taken from different stages in an aggregation reaction to the oligomer and fibril concentrations at the same time points, either measured directly or calculated using our model. Our study thus provides a window into the putative physiological functions of different classes of oligomers. In type B oligomers, the protein is likely trapped in conformations that do not allow them to reorganize to form a fibril-like oligomer. Due to the relatively slow dissociation time, the stable type B oligomers have a longer persistence time and hence have more potential to cause cellular damage than type A oligomers. Notably, we did not see any direct toxicity of these oligomeric preparations in cell culture,[15] but recent *in vitro* experiments have demonstrated that they can cause calcium influx into lipid vesicles and bind tightly to chaperones thus challenging the cell's quality control systems.[53] Although this study did not distinguish between different classes of oligomers, the sample was withdrawn at the peak of type B oligomer population, so it is likely that these effects are due to the more stable oligomeric species. Overload of the quality control systems may be connected to neurodegenerative diseases,[54,55] which underscores the importance of efficient chaperone sinks even if they are off-pathway to fibril formation.

METHODS

Protein Expression and Labeling. A synthetic gene encoding I260C/C291A/C322A tau K18 codon optimized for expression in *E. coli*[9] in a pJ414 vector was purchased from DNA2.0 (Menlo Park, CA). This construct enables site-specific fluorophore-labeling at cysteine 260 by removing the two native cysteine residues.[15] The ΔK280 mutation was introduced using Quikchange site-directed mutagenesis. Protein expression and purification was performed as described previously.[15] Before fluorophore labeling, the protein was incubated with 10 mM DTT in PBS for 30 min and subsequently buffer exchanged into degassed PBS using a CentriPure P25 column. A 1.5 molar excess of maleimide derivatives of either Alexa 488 or 647 (Molecular Probes) was added to tau typically with a concentration of 200−300 μM and allowed to react for 2 h at 37 °C. The reaction was quenched by addition of 10 mM DTT, and the monomeric protein was subsequently separated from unreacted dye and oligomeric species by gel filtration on a Superdex75 10−300 column. Tau K18 was concentrated to a concentration of 200−300 μM using a spin filter and frozen in liquid nitrogen in aliquots. Samples were used without refreezing of aliquots as this was found to cause preaggregation of the protein.

ThT Measurements and Seeding. Samples for ThT measurements were prepared from unlabeled protein in 50 mM ammonium acetate, pH 7, 1 mM DTT, and 20 μM ThT. Prior to the experiment, the sample was spun at 14000*g* for 5 min, and only the top two-thirds of the supernatant were used for the reaction to remove aggregated proteins, which is crucial to the reproducibility of the experiment. The reaction was started by addition of low molecular weight heparin (average MW = 5000, Fisher Scientific) at a molar ratio of one heparin to four tau. Multiple reactions were run in parallel in a 96-well plate (Corning 3881) using a sample volume of 60 μL. ThT was excited through a 440 nm/10 nm filter, and the fluorescence emission was selected with a 480 nm/10 nm filter. Measurements were done under quiescent conditions and at 37 °C. Aliquots were taken out from an aggregation reaction identical to that described above after 0, 15, 45, and 90 min of incubation and stored on ice until the last time point. Half the samples were spun for 5 min at 14000*g* to pellet fibrils. A 10% volume of the aliquots was added to new tau K18 ΔK280 aggregation reactions in 10 mM Na_2HPO_4/NaH_2PO_4, pH 7, 100 mM NaCl, 1 mM DTT, 20 mM ThT, 2.5 mM heparin. The ThT fluorescence was monitored as described above except the reaction was carried out at 30 °C.

Single-Molecule FRET Measurements. Aggregation reactions were carried out using a mixture of 5 μM tau−Alexa488 and 5 μM tau−Alexa647. The reaction was initiated by addition of heparin and aliquots were taken out as indicated and diluted 12.500 times before smFRET analysis. The diluted sample was pumped through a microfluidic channel[12,56] at a flow rate of 0.5 cm/min. A 488 nm laser beam was focused to a diffraction limited spot in the center of the channel by a 60× NA 1.4 microscope objective. Fluorescence emission was collected by the same objective and passed through a FF500/646-Di01 dichroic filter. The fluorescence emission was split

DOI: 10.1021/acschemneuro.8b00250
ACS Chem. Neurosci. 2018, 9, 3060−3071

into two channels by a FF605-Di02 dichroic filter, and selected with a 535/50 bandpass filter for the donor signal and FF01-697/75 filter for the acceptor. Photon counts were collected in 200 μs time bins for 6 min per time point.

Analysis of smFRET Data. Monomer and oligomer events were identified as time bins having more than 10 photons in the donor and acceptor channel, respectively. Photon counts were corrected for cross-talk and background fluorescence as described previously.[15] Concentrations were estimated by normalizing the burst rate relative to the known concentration of monomer in the first time-point. Bursts were classified as large if they had more than ten times the average burst count of a monomer event, which equals approximately 180 photons in total.

SAVE Experiments. SAVE experiments were performed as described previously.[21,22] In summary, borosilicate glass coverslips (VWR international, Ø 50 mm) were cleaned using an argon plasma cleaner (PDC-002, Harrick Plasma) for 30 min to remove any fluorescent residues. Multiwell slide chambers (CultureWell chambered cover glass 50 well, Grace Bio-Laboratories) were separated from the original cover glass and affixed to the cleaned cover slides. To stain aggregates for imaging, samples were diluted into 30 nM pFTAA to a final protein concentration of 25 nM tau. Then 10 μL of each sample was adsorbed to the cover slides for 15 min before imaging. The samples were imaged using a home-built total internal reflection fluorescence microscope as described previously.[22]

Quantitative Modeling at 27−42 °C. We developed a kinetic model of the aggregation reactions based on eqs 1−4. These equations may be solved exactly, yielding:

$$[S_A](t) = \frac{k_{oA}[m](0)}{k_{dA} - 2k_+\gamma}(e^{-2[P]k_+t} - e^{-k_{dA}t}) \quad (5)$$

$$[S_B](t) = \frac{k_{oB}[m](0)}{k_{dB} - 2k_+\gamma}(e^{-2[P]k_+t} - e^{-k_{dB}t}) \quad (6)$$

$$[m](t) = [m](0)\, e^{-2[P]k_+t}, \quad [m](t) + [M](t) = [m](0) \quad (7)$$

We observe a large k_{dA} in practice. We see that, if $k_{dA} \gg 2k_+\gamma$, monomers and type A oligomers are effectively in equilibrium after a short initial time, with equilibrium constant $K_E = k_{oA}/k_{dA}$. Indeed, above 32 °C formation and dissociation of type A oligomers occurs so rapidly that this occurs by the first time point and the rate constants k_{oA} and k_{dA} cannot be determined at all; we may instead only determine an average K_E over these 2 temperatures. All we may infer about the magnitudes of the component rate constants is that they are larger than those at 32 °C. At lower temperatures, this does not occur quite so rapidly; nonetheless, the transition time is still short enough that the rate constants cannot be determined with great accuracy. However, at any temperature we may infer from the form of eq 5 lower bounds for k_{dA} and therefore for k_{oA}. The data at 27−42 °C were fitted to the analytical expressions eqs 5−7 using code from the online fitting platform Amylofit;[27] and the best-fit rate constants were recorded (Table S1).

Quantitative Modeling at 22 °C. At 22 °C, new filament formation is slow enough that a lag phase is visible, and nucleation is no longer effectively instantaneous. We must modify our model to reproduce this behavior, yielding the following equations instead of eq 3:

$$\frac{d[P](t)}{dt} = k_c[S_A](t) \quad (8)$$

$$\frac{d[m](t)}{dt} = -2k_+[m](t)[P](t) \quad (9)$$

These equations are related to those employed in ref 40. The rate constants at 27 °C were used to develop trial parameters of sufficient accuracy to enable an efficient numerical fit of the 22 °C data to eqs 1, 2, 3, 8, and 9) to be carried out. The resultant rate constants for oligomer formation and dissociation may be directly compared with those determined at higher temperatures. In all cases, the fits were of high enough quality to verify the consistency of our model with the experimental data.

■ ASSOCIATED CONTENT

Supporting Information

The Supporting Information is available free of charge on the ACS Publications website at DOI: 10.1021/acschemneuro.8b00250.

Additional information about the selection and evaluation of kinetic modeling, kinetic rate constants determined from model fitting, and the effect of the heparin/tau ratio on bulk aggregation reactions (PDF)

■ AUTHOR INFORMATION

Corresponding Authors

*D.K. E-mail: dk10012@cam.ac.uk.
*T.P.J.K. E-mail: tpjk2@cam.ac.uk.

ORCID

Magnus Kjaergaard: 0000-0002-7020-9366
Franziska Kundel: 0000-0001-5013-0004
Georg Meisl: 0000-0002-6562-7715
Tuomas P. J. Knowles: 0000-0002-7879-0140

Present Address

[▽]F.K.: Cell Biology and Biophysics Unit, European Molecular Biology Laboratory, Heidelberg, Germany.

Author Contributions

[#]M.K. and A.J.D. contributed equally. M.K. and F.K. conducted experiments supervised by D.K. A.J.D. and G.M. performed modeling under supervision of T.P.J.K. S.Q. provided key materials. The manuscript was written through contributions of all authors. All authors have given approval to the final version of the manuscript.

Funding

D.K. acknowledges funding from the Royal Society and ERC Advanced Grant (669237). M.K. acknowledges fellowships from the Danish Research Council and the Lundbeck Foundation (R165-2013-15269). A.J.D. acknowledges a studentship from the Schiff Foundation. G.M. acknowledges a fellowship from Sidney Sussex College, Cambridge. T.P.J.K. acknowledges financial support from the Wellcome Trust, the Cambridge Centre for Misfolding Diseases, the BBSRC, and the Frances and Augustus Newman foundation. The research leading to these results has received funding from the European Research Council under the European Union's Seventh Framework Programme (FP7/2007-2013) through the ERC grant PhysProt (Agreement No. 337969) and the COFUND programme (Agreement No. 609033).

Notes

The authors declare no competing financial interest.

■ REFERENCES

(1) Knowles, T. P. J., Vendruscolo, M., and Dobson, C. M. (2014) The amyloid state and its association with protein misfolding diseases. *Nat. Rev. Mol. Cell Biol. 15*, 384−96.

(2) Arriagada, P. V., Growdon, J. H., Hedley-Whyte, E. T., and Hyman, B. T. (1992) Neurofibrillary Tangles But Not Senile Plaques Parallel Duration and Severity of Alzheimers-Disease. *Neurology 42*, 631−639.

(3) Avila, J., Lucas, J. J., Perez, M., and Hernandez, F. (2004) Role of Tau Protein in Both Physiological and Pathological Conditions. *Physiol. Rev. 84*, 361−384.

DOI: 10.1021/acschemneuro.8b00250
ACS Chem. Neurosci. 2018, 9, 3060−3071

(4) Fitzpatrick, A. W. P., Falcon, B., He, S., Murzin, A. G., Murshudov, G., Garringer, H. J., Crowther, R. A., Ghetti, B., Goedert, M., and Scheres, S. H. W. (2017) Cryo-EM structures of tau filaments from Alzheimer ' s disease. *Nature 547*, 185−190.
(5) Wischik, C. M., Novak, M., Thøgersen, H. C., Edwards, P. C., Runswick, M. J., Jakes, R., Walker, J. E., Milstein, C., Roth, M., and Klug, a. (1988) Isolation of a fragment of tau derived from the core of the paired helical filament of Alzheimer disease. *Proc. Natl. Acad. Sci. U. S. A. 85*, 4506−4510.
(6) Goedert, M., Crowther, A. R., and Spillantini, M. G. (1998) Tau Mutations Cause Frontotemporal Dementias. *Neuron 21*, 955−958.
(7) Rizzu, P., Van Swieten, J. C., Joosse, M., Hasegawa, M., Stevens, M., Tibben, A., Niermeijer, M. F., Hillebrand, M., Ravid, R., Oostra, B. A., Goedert, M., van Duijn, C. M., and Heutink, P. (1999) High Prevalence of Mutations in the Microtubule-Associated Protein Tau in a Population Study of Frontotemporal Dementia in the Netherlands. *Am. J. Hum. Genet. 64*, 414−421.
(8) Alonso, A. d. C., Grundke-Iqbal, I., and Iqbal, K. (1996) Alzheimer's disease hyperphosphorylated tau sequesters normal tau into tangles of filaments and dissassembles microtubules. *Nat. Med. 2*, 783−787.
(9) Perry, G., Siedlak, S. L., Richey, P., Kawai, M., Cras, P., Kalaria, R. N., Galloway, P. G., Scardina, J. M., Cordell, B., and Greenberg, B. D. (1991) Association of heparan sulfate proteoglycan with the neurofibrillary tangles of Alzheimer's disease. *J. Neurosci. 11*, 3679−3683.
(10) Cremades, N., Cohen, S. I. A., Deas, E., Abramov, A. Y., Chen, A. Y., Orte, A., Sandal, M., Clarke, R. W., Dunne, P., Aprile, F. A., Bertoncini, C. W., Wood, N. W., Knowles, T. P. J., Dobson, C. M., and Klenerman, D. (2012) Direct Observation of the Interconversion of Normal and Toxic Forms of α-Synuclein. *Cell 149*, 1048−59.
(11) Paslawski, W., Mysling, S., Thomsen, K., Jørgensen, T. J. D., and Otzen, D. E. (2014) Co-existence of two different α-synuclein oligomers with different core structures determined by hydrogen/deuterium exchange mass spectrometry. *Angew. Chem., Int. Ed. 53*, 7560−7563.
(12) Tosatto, L., Horrocks, M. H., Dear, A. J., Knowles, T. P. J., Dalla Serra, M., Cremades, N., Dobson, C. M., and Klenerman, D. (2015) Single-molecule FRET studies on alpha-synuclein oligomerization of Parkinson's disease genetically related mutants. *Sci. Rep. 5*, 16696.
(13) Iljina, M., Garcia, G. A., Horrocks, M. H., Tosatto, L., Choi, M. L., Ganzinger, K. A., Abramov, A. Y., Gandhi, S., Wood, N. W., Cremades, N., Dobson, C. M., Knowles, T. P. J., and Klenerman, D. (2016) Kinetic model of the aggregation of alpha-synuclein provides insights into prion-like spreading. *Proc. Natl. Acad. Sci. U. S. A. 113*, E1206−E1215.
(14) Kayed, R. (2003) Common Structure of Soluble Amyloid Oligomers Implies Common Mechanism of Pathogenesis. *Science (Washington, DC, U. S.) 300*, 486−489.
(15) Shammas, S. L., Garcia, G. A., Kumar, S., Kjaergaard, M., Horrocks, M. H., Shivji, N., Mandelkow, E., Knowles, T. P. J., Mandelkow, E., and Klenerman, D. (2015) A mechanistic mode of tau amyloid aggregation based on direct observation of oligomers. *Nat. Commun. 6*, 7025.
(16) Orte, A., Birkett, N. R., Clarke, R. W., Devlin, G. L., Dobson, C. M., and Klenerman, D. (2008) Direct characterization of amyloidogenic oligomers by single-molecule fluorescence. *Proc. Natl. Acad. Sci. U. S. A. 105*, 14424−9.
(17) Kampers, T., Friedhoff, P., Biernat, J., Mandelkow, E., and Mandelkow, E.-M. (1996) RNA stimulates aggregation of microtubule-associated protein tau into Alzheimer-like paired helical filaments. *FEBS Lett. 399*, 344−349.
(18) Goedert, M., Jakes, R., Spillantini, M. G., Hasegawa, M., Smith, M. J., and Crowther, R. A. (1996) Assembly of microtubule-associated protein tau into Alzheimer-like filaments induced by sulphated glycosaminoglycans. *Nature 383*, 550−553.
(19) Ramachandran, G., and Udgaonkar, J. B. (2011) Understanding the kinetic roles of the inducer heparin and of rod-like protofibrils during amyloid fibril formation by Tau protein. *J. Biol. Chem. 286*, 38948−59.
(20) Glabe, C. G. (2008) Structural classification of toxic amyloid oligomers. *J. Biol. Chem. 283*, 29639−29643.
(21) Horrocks, M. H., Lee, S. F., Gandhi, S., Magdalinou, N. K., Chen, S. W., Devine, M. J., Tosatto, L., Kjaergaard, M., Beckwith, J. S., Zetterberg, H., Iljina, M., Cremades, N., Dobson, C. M., Wood, N. W., and Klenerman, D. (2016) Single-molecule imaging of individual amyloid protein aggregates in human biofluids. *ACS Chem. Neurosci. 7*, 399−406.
(22) Kundel, F., Hong, L., Falcon, B., McEwan, W., Michaels, T. C. T., Meisl, G., Esteras, N., Abramov, A. Y., Knowles, T. P. J., Goedert, M., and Klenerman, D. (2018) Measurement of tau filament fragmentation provides insights into prion-like spreading. *ACS Chem. Neurosci. 9*, 1276.
(23) Klingstedt, T., Shirani, H., Åslund, K. O. A., Cairns, N. J., Sigurdson, C. J., Goedert, M., and Nilsson, K. P. R. (2013) The structural basis for optimal performance of oligothiophene-based fluorescent amyloid ligands: Conformational flexibility is essential for spectral assignment of a diversity of protein aggregates. *Chem. - Eur. J. 19*, 10179−10192.
(24) Knowles, T. P. J., Waudby, C. A., Devlin, G. L., Cohen, S. I. A., Aguzzi, A., Vendruscolo, M., Terentjev, E. M., Welland, M. E., and Dobson, C. M. (2009) An Analytical Solution to the Kinetics. *Science (Washington, DC, U. S.) 326*, 1533−1537.
(25) Meisl, G., Yang, X., Hellstrand, E., Frohm, B., Kirkegaard, J. B., Cohen, S. I. A., Dobson, C. M., Linse, S., and Knowles, T. P. J. (2014) Differences in nucleation behavior underlie the contrasting aggregation kinetics of the Aβ40 and Aβ42 peptides. *Proc. Natl. Acad. Sci. U. S. A. 111*, 9384−9389.
(26) Cohen, S. I. A., Linse, S., Luheshi, L. M., Hellstrand, E., White, D. A., Rajah, L., Otzen, D. E., Vendruscolo, M., Dobson, C. M., and Knowles, T. P. J. (2013) Proliferation of amyloid- 42 aggregates occurs through a secondary nucleation mechanism. *Proc. Natl. Acad. Sci. U. S. A. 110*, 9758−9763.
(27) Meisl, G., Kirkegaard, J. B., Arosio, P., Michaels, T. C. T., Vendruscolo, M., Dobson, C. M., Linse, S., and Knowles, T. P. J. (2016) Molecular mechanisms of protein aggregation from global fitting of kinetic models. *Nat. Protoc. 11*, 252−272.
(28) Pham, C. L. L., Rey, A., Lo, V., Soulès, M., Ren, Q., Meisl, G., Knowles, T. P. J., Kwan, A. H., and Sunde, M. (2016) Self-assembly of MPG1, a hydrophobin protein from the rice blast fungus that forms functional amyloid coatings, occurs by a surface-driven mechanism. *Sci. Rep. 6*, 25288.
(29) Šarić, A., Michaels, T. C. T., Zaccone, A., Knowles, T. P. J., and Frenkel, D. (2016) Kinetics of spontaneous filament nucleation via oligomers: Insights from theory and simulation. *J. Chem. Phys. 145*, 211926.
(30) Berglund, N. Kramers' law: Validity, derivations and generalisations. *arXiv*, 2011, 1106.5799v2, https://arxiv.org/abs/1106.5799.
(31) Schuler, B., Lipman, E. a, and Eaton, W. a. (2002) Probing the free-energy surface for protein folding with single-molecule fluorescence spectroscopy. *Nature 419*, 743−748.
(32) Onuchic, J. N., Luthey-Schulten, Z., and Wolynes, P. G. (1997) THEORY OF PROTEIN FOLDING: The Energy Landscape Perspective. *Annu. Rev. Phys. Chem. 48*, 545−600.
(33) Kramers, H. A. (1940) Brownian Motion in a Field of Force and the Diffusion Model. *Physica 7*, 284−304.
(34) Zwanzig, R. (1997) Two-state models of protein folding kinetics. *Proc. Natl. Acad. Sci. U. S. A. 94*, 148−50.
(35) Buell, A. K., Blundell, J. R., Dobson, C. M., Welland, M. E., Terentjev, E. M., and Knowles, T. P. J. (2010) Frequency factors in a landscape model of filamentous protein aggregation. *Phys. Rev. Lett. 104*, 228101.
(36) Buell, A. K., Dhulesia, A., White, D. A., Knowles, T. P. J., Dobson, C. M., and Welland, M. E. (2012) Detailed Analysis of the Energy Barriers for Amyloid Fibril Growth. *Angew. Chem., Int. Ed. 51*, 5247−5251.

DOI: 10.1021/acschemneuro.8b00250
ACS Chem. Neurosci. 2018, 9, 3060−3071

(37) Cohen, S. I. A., Cukalevski, R., Michaels, T. C. T., Šarić, A., Törnquist, M., Vendruscolo, M., Dobson, C. M., Buell, A. K., Knowles, T. P. J., and Linse, S. (2018) Distinct thermodynamic signatures of oligomer generation in the aggregation of the amyloid-β peptide. *Nat. Chem. 10*, 523.
(38) Lee, S. J. C., Nam, E., Lee, H. J., Savelieff, M. G., and Lim, M. H. (2017) Towards an understanding of amyloid-β oligomers: characterization, toxicity mechanisms, and inhibitors. *Chem. Soc. Rev. 46*, 310−323.
(39) Danzer, K. M., Haasen, D., Karow, A. R., Moussaud, S., Habeck, M., Giese, A., Kretzschmar, H., Hengerer, B., and Kostka, M. (2007) Different Species of -Synuclein Oligomers Induce Calcium Influx and Seeding. *J. Neurosci. 27*, 9220−9232.
(40) Yang, J., Dear, A. J., Michaels, T. C. T., Dobson, C. M., Knowles, T. P. J., Wu, S., and Perrett, S. (2018) Direct Observation of Oligomerization by Single Molecule Fluorescence Reveals a Multistep Aggregation Mechanism for the Yeast Prion Protein Ure2. *J. Am. Chem. Soc. 140*, 2493−2503.
(41) Ramachandran, G., and Udgaonkar, J. B. (2011) Understanding the kinetic roles of the inducer heparin and of rod-like protofibrils during amyloid fibril formation by tau protein. *J. Biol. Chem. 286*, 38948−38959.
(42) Buell, A. K., Dhulesia, A., White, D. A., Knowles, T. P. J., Dobson, C. M., and Welland, M. E. (2012) Detailed analysis of the energy barriers for amyloid fibril growth. *Angew. Chem., Int. Ed. 51*, 5247−5251.
(43) Zhu, H.-L., Fernández, C., Fan, J.-B., Shewmaker, F., Chen, J., Minton, A. P., and Liang, Y. (2010) Quantitative characterization of heparin binding to Tau protein: implication for inducer-mediated Tau filament formation. *J. Biol. Chem. 285*, 3592−9.
(44) Mukrasch, M. D., Biernat, J., Von Bergen, M., Griesinger, C., Mandelkow, E., and Zweckstetter, M. (2005) Sites of tau important for aggregation populate β-structure and bind to microtubules and polyanions. *J. Biol. Chem. 280*, 24978−24986.
(45) Mukrasch, M. D., Bibow, S., Korukottu, J., Jeganathan, S., Biernat, J., Griesinger, C., Mandelkow, E., and Zweckstetter, M. (2009) Structural polymorphism of 441-residue Tau at single residue resolution. *PLoS Biol. 7*, e1000034.
(46) Ozenne, V., Schneider, R., Yao, M., Huang, J., Salmon, L., Zweckstetter, M., Jensen, M. R., and Blackledge, M. (2012) Mapping the Potential Energy Landscape of Intrinsically Disordered Proteins at Amino Acid Resolution. *J. Am. Chem. Soc. 134*, 15138−15148.
(47) Galvagnion, C., Buell, A. K., Meisl, G., Michaels, T. C. T., Vendruscolo, M., Knowles, T. P. J., and Dobson, C. M. (2015) Lipid vesicles trigger α-synuclein aggregation by stimulating primary nucleation. *Nat. Chem. Biol. 11*, 229−234.
(48) Brown, J. W. P., Buell, A. K., Michaels, T. C. T., Meisl, G., Carozza, J., Flagmeier, P., Vendruscolo, M., Knowles, T. P. J., Dobson, C. M., and Galvagnion, C. (2016) β-Synuclein suppresses both the initiation and amplification steps of α-synuclein aggregation via competitive binding to surfaces. *Sci. Rep. 6*, 36010.
(49) Elbaum-Garfinkle, S., Ramlall, T., and Rhoades, E. (2010) The role of the lipid bilayer in tau aggregation. *Biophys. J. 98*, 2722−2730.
(50) Georgieva, E. R., Xiao, S., Borbat, P. P., Freed, J. H., and Eliezer, D. (2014) Tau binds to lipid membrane surfaces via short amphipathic helices located in its microtubule-binding repeats. *Biophys. J. 107*, 1441−1452.
(51) Knowles, T. P. J., White, D. A., Abate, A. R., Agresti, J. J., Cohen, S. I. A., Sperling, R. A., De Genst, E. J., Dobson, C. M., and Weitz, D. A. (2011) Observation of spatial propagation of amyloid assembly from single nuclei. *Proc. Natl. Acad. Sci. U. S. A. 108*, 14746−14751.
(52) Cohen, S. I. A., Rajah, L., Yoon, C. H., Buell, A. K., White, D. A., Sperling, R. A., Vendruscolo, M., Terentjev, E. M., Dobson, C. M., Weitz, D. A., and Knowles, T. P. J. (2014) Spatial propagation of protein polymerization. *Phys. Rev. Lett. 112*, 098101.
(53) Kundel, F., De, S., Flagmeier, P., Horrocks, M. H., Kjaergaard, M., Shammas, S. L., Jackson, S. E., Dobson, C. M., and Klenerman, D. (2018) Hsp70 Inhibits the Nucleation and Elongation of Tau and Sequesters Tau Aggregates with High Affinity. *ACS Chem. Biol. 13*, 636−646.
(54) Muchowski, P. J., and Wacker, J. L. (2005) Modulation of neurodegeneration by molecular chaperones. *Nat. Rev. Neurosci. 6*, 11−22.
(55) Morimoto, R. I. (2008) Proteotoxic stress and inducible chaperone networks in neurodegenerative disease and aging. *Genes Dev. 22*, 1427−1438.
(56) Horrocks, M. H., Li, H., Shim, J.-U., Ranasinghe, R. T., Clarke, R. W., Huck, W. T. S., Abell, C., and Klenerman, D. (2012) Single molecule fluorescence under conditions of fast flow. *Anal. Chem. 84*, 179−85.

DOI: 10.1021/acschemneuro.8b00250
ACS Chem. Neurosci. 2018, 9, 3060−3071